CHALMERS

CPL

Chalmers Publication Library

Institutional Repository of
Chalmers University of Technology
http://publications.lib.chalmers.se

Copyright notice (preprint)

This is a preprint of an article whose final and definitive form has been published in *Nuclear Instruments & Methods in Physics Research Section B-Beam Interactions with Materials and Atoms* [2011] [Copyright Elsevier]; *Nuclear Instruments & Methods in Physics Research Section B-Beam Interactions with Materials and Atoms* is available online at:
http://dx.doi.org/10.1016/j.nimb.2011.01.004

Application of Combined Neutron Diffraction and Impedance Spectroscopy for *In-situ* Structure and Conductivity Studies of $La_2Mo_2O_9$

Jingjing Liu [a], Stephen. Hull [b], Istaq Ahmed [b,c], Stephen J. Skinner [a, *]

[a] *Department of Materials, Imperial College London, Prince Consort Road, London SW7 2BP, UK*

[b] *The ISIS facility, Rutherford Appleton Laboratory, Chilton, Didcot, Oxfordshire, OX11 0QX, UK*

[c] *Department of Chemical and Biological Engineering, Chalmers University of Technology, SE-412 96 Gothenburg, Sweden*

Abstract: *In-situ* neutron diffraction combined with AC impedance spectroscopy was applied successfully to investigate the correlation between crystal structure and electrical properties of the $La_2Mo_2O_9$ oxide ion conducting electrolyte material. Neutron diffraction patterns were collected as a function of temperature while the AC impedance spectra were recorded simultaneously using a modified sample environment to monitor the conductivity change of the sample. A close relationship between unit cell parameters and the bulk conductivity was observed, confirming that the oxygen transport is dependent on the lattice structure. With the transition from the low temperature alpha to the high temperature beta phase, the crystal structure released more space for oxygen transport, leading to a dramatic increase of the ionic conductivity. The successful application of this technique provides a new method to simultaneously investigate crystal structure and electrical properties in electro-ceramics in the future.

Keywords: In-situ; Neutron diffraction; impedance spectroscopy; $La_2Mo_2O_9$; electrolyte

---

[*] Corresponding author: Stephen J. Skinner, Department of Materials, Imperial College London, Prince Consort Road, London, UK, SW7 2BP. Tel: +44 (0)20 7594 6782 Fax: +44 (0)20 7594 6757

Email address: s.skinner@imperial.ac.uk

1. Introduction

$La_2Mo_2O_9$ has been studied extensively as a promising electrolyte material for Solid Oxide Fuel Cells (SOFCs) [1-3]. It is well known that the material undergoes a phase transition at 580˚C from α-$La_2Mo_2O_9$ at low temperature to β-$La_2Mo_2O_9$ at high temperature, with a conductivity increase of about two orders of magnitude [1]. Studies of the crystal structure have shown that the nature of the phase transition is a change of the distribution of oxygen defects, from long-range order to dynamic, short-range order [4, 5]. The high temperature phase can be indexed as a cubic structure, and it is indicated to be a time-averaged version of the low temperature phase, the monoclinic structure. The oxygen transport mechanism changes with the phase transition from a thermally activated Arrhenius type at low temperature to a thermally assisted VTF (Vogel-Tamman-Fulcher) type [2]. The increase of the ionic conductivity is believed to be due to a volume expansion in the unit cell. The released extra free volume is likely to favour the mobility of oxygen ions, which is the explanation for the Arrhenius-VTF transition [6].

Neutron diffraction is widely employed to study complex oxide crystal structures, compared to the conventional laboratory X-ray diffraction, especially when a full pattern refinement is required to obtain high quality crystallographic data. For *in-situ* studies of structural changes using neutron diffraction there are two main modes of operation possible: constant wavelength or time-of-flight (TOF). Each has distinct advantages/disadvantages, and of course the individual instrument design dictates many of the key parameters for high quality structure determination. TOF neutron diffraction has been adopted in this work due to its rapid characterization of structures, rapid collection of data and allowance of complex sample environment. *In-situ* neutron diffraction has been applied to investigate the crystal structure change of

$La_2Mo_2O_9$ during the phase transition, especially the expansion of lattice parameters and unit cell volume [6, 7]. Based upon the structure analysis, it is important to relate the crystalline structure to the electrical properties, in order to understand the oxygen transport mechanism. However to date there have been no studies that correlate the phase transition with functional properties through combined *in-situ* structural and conductivity measurements. Indeed there are only limited examples of this concept having been applied to conducting samples.

The purpose of this work was to develop a new experimental technique which can combine *in-situ* neutron diffraction with simultaneous AC impedance spectroscopy for electrical conductivity measurement. Therefore, both crystal structure and conductivity can be obtained simultaneously, from which a direct correlation between the two can be acquired.

2. Experimental

$La_2Mo_2O_9$ powder was synthesized by the solid state route, which has been detailed in a previous report [8]. To measure AC impedance spectra a dense pellet sample is needed and to ensure that the neutron beam can penetrate the entire sample with good data statistics a larger sample is required. Therefore in this work, a sample with a diameter of 10.8 mm and a thickness of 5.0 mm was prepared by cold uni-axial and iso-static pressing followed by sintering at 1100˚C. As electrodes, platinum paste was applied to both sides of the sample which was then heated at 800˚C for 1 hour to ensure good adherence of the electrical contact.

The instrument used to collect neutron diffraction data was the POLARIS diffractometer at the ISIS facility (Rutherford Appleton Laboratory, UK). Data from the backscattering detectors were used in this work (130~160˚, 2θ) [9]. The

measurements were performed at variable temperatures (ranging from 500˚C to 640˚C, covering the phase transition region), using a vanadium furnace with the sample held under a static air atmosphere in the closed sample environment.

In-situ AC impedance measurements were carried out in static air in the frequency range of 5 MHz~0.1 Hz with an AC amplitude of 100 mV using a Solartron 1260 Frequency Response Analyser (FRA). The impedance measurement rig, as illustrated in Fig. 1, designed and built at ISIS, was mounted vertically in the furnace which was put in the sample tank. The neutron diffraction data were recorded on the middle of the sample to avoid collecting additional diffraction data from the platinum electrodes on both sides of the pellet.

The sample was held at each temperature for 2 hours for thermal equilibration, during which period neutron diffraction data collection was conducted and several impedance spectra were collected to observe any change of the resistance during the equilibration. 2 hours was also the minimum time required to obtain good quality neutron diffraction data.

After the *in-situ* diffraction and conductivity measurement, an AC impedance measurement was also conducted on the same sample in the laboratory at Imperial College London under a static air atmosphere using the same AC impedance instrument with an applied potential of 50 mV in the frequency range of 13 MHz ~ 0.1 Hz, in order to verify the conductivity obtained from the *in-situ* experiment.

In the current study, the correlation between lattice parameters and the conductivities during the phase transition region was investigated. As the structure of both α and β $La_2Mo_2O_9$ has previously been reported, only the Le Bail method [10] was applied to extract lattice parameters from neutron diffraction patterns. Without refining the structure factors F_{hkl} of all atoms in the unit cell which includes atom

positions, scattering factors, atomic site occupation and thermal factors, the Le Bail method estimates reflection intensities by refining unit cell parameters, background, peak shape and diffractometer parameters. It yields the best possible intensity values and optimal experimental parameters (background, unit cell *etc*). The Le Bail extraction was performed using GSAS (General Structure Analysis System) + EXPGUI software [11, 12]. Diffraction patterns were analysed by comparison with the previously reported structural models for α-$La_2Mo_2O_9$ and β-$La_2Mo_2O_9$ [4, 13]. The extracted unit cell parameters were correlated with the conductivity variations during the heating and cooling stages.

3. Results and Discussion

Fig. 2 presents two neutron diffraction patterns of $La_2Mo_2O_9$ recorded at 560˚C and 580˚C when the material exists as the two different phases. The pattern collected at 580˚C is indexed as a cubic structure in agreement with literature reports [13]. Clearly, at 560˚C the diffraction data for α-$La_2Mo_2O_9$ indicates a lower symmetry than that for β-$La_2Mo_2O_9$ recorded at 580˚C. The disappearance of the small extra peaks (as indicated by * in Fig. 2) and the sharpening of peaks labelled as (123), (122) and (112) when the temperature is increased to 580˚C suggests a transformation from the monoclinic superstructure to a cubic phase, as expected from the literature reports [1].

A typical impedance spectrum from the *in-situ* measurement is displayed in Fig. 3. As can be seen in the figure, the high-frequency arc, normally attributed to the grain bulk, is not present in the spectrum. Each data set recorded has been fitted to an equivalent circuit model, attributing capacitance and resistance to each of the spectral components. Detailed discussion of the analysis of impedance spectra is given elsewhere [14]. In the fitted equivalent circuit in Fig 3 (inset) the value of *R1* is taken

as the bulk resistance, while *R2* is the grain boundary resistance. *R3* and *R4* are resistances from interface and electrode components respectively. A full analysis of the impedance spectra is reported elsewhere [15] and from these data it is a simple process to extract the conductivity values for the sample. Fig. 4 presents the conductivities obtained from both the simultaneous *in-situ* diffraction and conductivity measurements and the *ex-situ* impedance measurement. The data from the simultaneous *in-situ* measurements are consistent with the conductivity results obtained during both heating and cooling stages recorded *ex-situ* at Imperial College, implying that the conductivity results obtained simultaneously with the collection of neutron diffraction patterns are reliable despite the complex experimental environment.

A Le Bail extraction was performed on each of the diffraction patterns and the obtained lattice parameters at different temperatures are listed in Table 1. The goodness-of-fit (χ^2) for each diffraction pattern is below 5 and the R_{wp} values are around 5.0%, even for the alpha phase which is indexed as a monoclinic superstructure, which indicates that the fitting results are good. The thermal evolution of the lattice parameters are presented in Fig. 5. As can be observed, the unit cell parameters increase nearly linearly when the temperature is increased. For the alpha phase, the increases of lattice parameters *a* and *b* follow the same trend line, while the parameter *c* is smaller than *a* and *b*, showing less dramatic increase with the temperature. The reason is probably that during the increase of the temperature, the unit cell is transforming to a cubic structure with the tilting of the monoclinic angle, which leads to a slower change in *c* axis direction. The β angle for the alpha phase remains constant in the low temperature range which is roughly 90.4˚, consistent with the published crystallographic details for α-$La_2Mo_2O_9$ [4].

The correlation between the unit cell volume and the conductivity is demonstrated in Fig. 6. An important increase of the unit cell volume (about 0.4%) is observed when the structure transforms to the cubic phase, which corresponds with the increase of the conductivity. Note that the bulk conductivity is presented here in order to show the correlation between the unit cell volume and the electrical property more clearly because the grain boundary contribution plays a dominant role in the total conductivity which is probably caused by impurity segregation along the grain boundaries. This observation supports the previous hypothesis that the extra volume expansion which originates from a unit cell tilting mechanism induces an increase of oxygen mobility in the structure. The relationship between the structural framework with the anionic conduction properties has been studied by a mathematical analysis [6]. However, the direct experimental observation of the correlation is made for the first time in the current work.

The structural change and electrical properties of $La_2Mo_2O_9$ were studied in detail for the phase transition. A cycle of cooling and heating in the temperature range of 580-560˚C was carried out with a step size of 10˚C for cooling and 5˚C for heating respectively. The Arrhenius plot of the bulk conductivity and the unit cell volume change during different temperature stages are displayed in Fig. 7 (a) and (b). Both the electrical property and the unit cell structure are fully reversible during cooling. However, a hysteresis phenomenon has been observed in both of the plots, which again testified the correlation between unit cell volume and electrical property. The hysteresis loop in $La_2Mo_2O_9$ has been previously reported in thermal analysis [1] and temperature dependence of dielectric permittivity [16], demonstrating that the phase transition in $La_2Mo_2O_9$ is a first-order transition. However, in this work, the hysteretic

behaviour in bulk conductivity and unit cell evolution as a function of temperature has been presented for the first time.

4. Conclusions

In this work, *in-situ* neutron diffraction and AC impedance measurements were successfully conducted. The AC impedance rig was designed to fit in the neutron diffractometer, and by comparing the obtained conductivity from the *in-situ* diffraction and conductivity measurement to the data from AC impedance measurement afterwards, the consistency between the two sets of data demonstrates the feasibility of applying *in-situ* neutron diffraction and conductivity measurement to solid state ionic materials.

The neutron diffraction patterns clearly demonstrate the change of the crystal structure of $La_2Mo_2O_9$ between alpha and beta phases, as shown by splitting and broadening of several peaks such as (123) (122) and (112). The close relationship between unit cell parameters and the bulk conductivity of $La_2Mo_2O_9$ suggests the fast oxygen transport is dependent on the opening of the unit cell.

Further work is required to optimize the *in-situ* diffraction and conductivity experimental system. Time resolved measurements are also required to record neutron diffraction data in order to detect the rapid structure change in a relatively short time period. The technique can be used to investigate the correlation between crystal structure and electrical properties in electro-ceramics in the future.

Acknowledgement

The authors would like to thank Lee Family for funding the studentship (Jingjing Liu) and STFC for funding the beam time at ISIS.

References

1. Lacorre P., Goutenoire F., Bohnke O., *Nature*, 2000, 404: 856-858.
2. Georges S., Goutenoire F., Bohnke O., Steil M. C., Skinner S. J., Wiemhofer H. D., Lacorre P., *J. New Mater. Electrochem. Syst.* , 2004, 7(1): 51-57.
3. Marrero-López D., Canales-Vázquez J., Ruiz-Morales J. C., Rodríguez A., Irvine J. T. S., Núñez P., *Solid State Ionics*, 2005, 176(23-24): 1807-1816.
4. Evans I. R., Howard J. A. K., Evans J. S. O., *Chem. Mater.*, 2005, 17(16): 4074-4077.
5. Malavasi L., Kim H. J., Billinge S. J. L., Proffen T., Tealdi C., Flor G., *J. Am. Chem. Soc.*, 2007, 129: 6903-6907.
6. Lacorre P., Selmi A., Corbel G., Boulard B., *Inorganic Chem.*, 2006, 45(2): 627-635.
7. Marrero-López D., Canales-Vázquez J., Zhou W. Z., Irvine J. T. S., Núñez P., *J. Solid State Chem.*, 2006, 179(1): 278-288.
8. Liu J., Chater R. J., Hagenhoff B., Morris R. J. H., Skinner S. J., *Solid State Ionics*, 2010, In press (doi:10.1016/j.ssi.2010.04.009).
9. Hull S.; Smith R. I.; David W. I. F.; Hannon A. C.; Mayers J.; Cywinski R. *Physica B* **1992**, *180-181*, 1000-100210. Le Bail A., Duroy H., Fourquet J. L., *Mater. Res. Bull.*, 1988, 23: 447-452.
11. Larson A. C., Von Dreele R. B., *General structure analysis system (GSAS)*. 1994, Los Alamos National Laboratory Report
12. Toby B. H., *J. Appl. Cryst.*, 2001, 34: 210-213.
13. Goutenoire F., Isnard O., Retoux R., Lacorre P., *Chem. Mater.*, 2000, 12(9): 2575-2580.
14. Irvine J. T. S., Sinclair D. C., West A. R., *Adv. Mater.*, 1990, 2(3): 132-138.
15. Liu J., *Mass transport and electrochemical properties of $La_2Mo_2O_9$ as a fast ionic conductor*. Department of Materials. Imperial College London. PhD. 2010, London
16. Khadasheva Z. S., Venskovskii N. U., Safronenko M. G., Mosunov A. V., Politova E. D., Stefanovich S. Y., *Inorganic Mater.*, 2002, 38(11): 1168-1171.

Figure Captions

Fig. 1 Schematic diagram of the designed AC impedance rig for the in-situ neutron diffraction environment

Fig. 2 Time-of-flight neutron diffraction patterns of α- and β-$La_2Mo_2O_9$ at 560˚C and 580˚C. *indicates additional peaks attributed to the monoclinic phase

Fig. 3 A typical AC impedance spectrum from the *in-situ* diffraction and conductivity measurement collected at 600˚C

Fig. 4 Comparison of total conductivities between the *in-situ* diffraction and conductivity measurement and the impedance measurement in the lab of the same $La_2Mo_2O_9$ sample

Fig. 5 Thermal evolution of the lattice parameters of $La_2Mo_2O_9$ during heating

Fig. 6 The correlation between the unit cell volume and the bulk conductivity

Fig. 7 Arrhenius plot of the bulk conductivity (a) the unit cell volume change (b) of the $La_2Mo_2O_9$ sample during different temperature stages.

Table Caption

Table 1 Lattice parameters of $La_2Mo_2O_9$ indexed as monoclinic superstructure and cubic below and above the phase transition temperature, respectively.

Table 1

Temp(˚C)	Phase	Lattice parameters (Å)			β (˚)	V (Å^3)	χ^2	R_{wp}
		a	*b*	*c*				
RT	alpha	14.311(2)	21.461(1)	28.577(2)	90.364(4)	8776.4(1)	3.99	5.1%
500	alpha	14.406(2)	21.613(2)	28.784(4)	90.362(5)	8962.1(2)	5.21	6.0%
520	alpha	14.412(2)	21.620(2)	28.790(4)	90.361(5)	8970.2(2)	5.07	5.9%
540	alpha	14.423(1)	21.627(1)	28.790(2)	90.397(3)	8980.3(1)	2.26	3.9%
560	alpha	14.426(1)	21.650(1)	28.798(2)	90.385(3)	8993.6(1)	2.44	4.1%
580	beta	7.220(3)	-	-	90	376.37(3)	2.04	3.7%
600	beta	7.223(4)	-	-	90	376.82(4)	3.30	4.7%
620	beta	7.227(3)	-	-	90	377.44(3)	2.12	3.8%
640	beta	7.230 (4)	-	-	90	377.96(3)	2.45	4.1%

Fig. 1

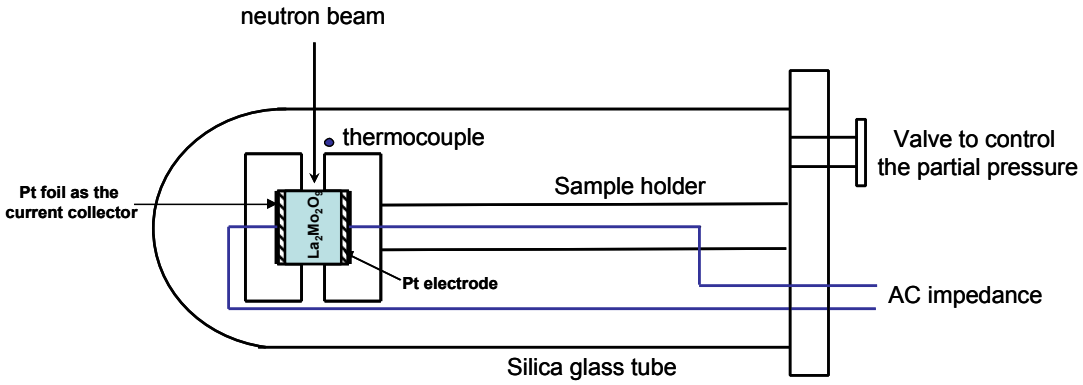
neutron beam
thermocouple
Valve to control
the partial pressure
Pt foil as the
current collector
Sample holder
$La_2Mo_2O_9$
Pt electrode
AC impedance
Silica glass tube

Fig. 2

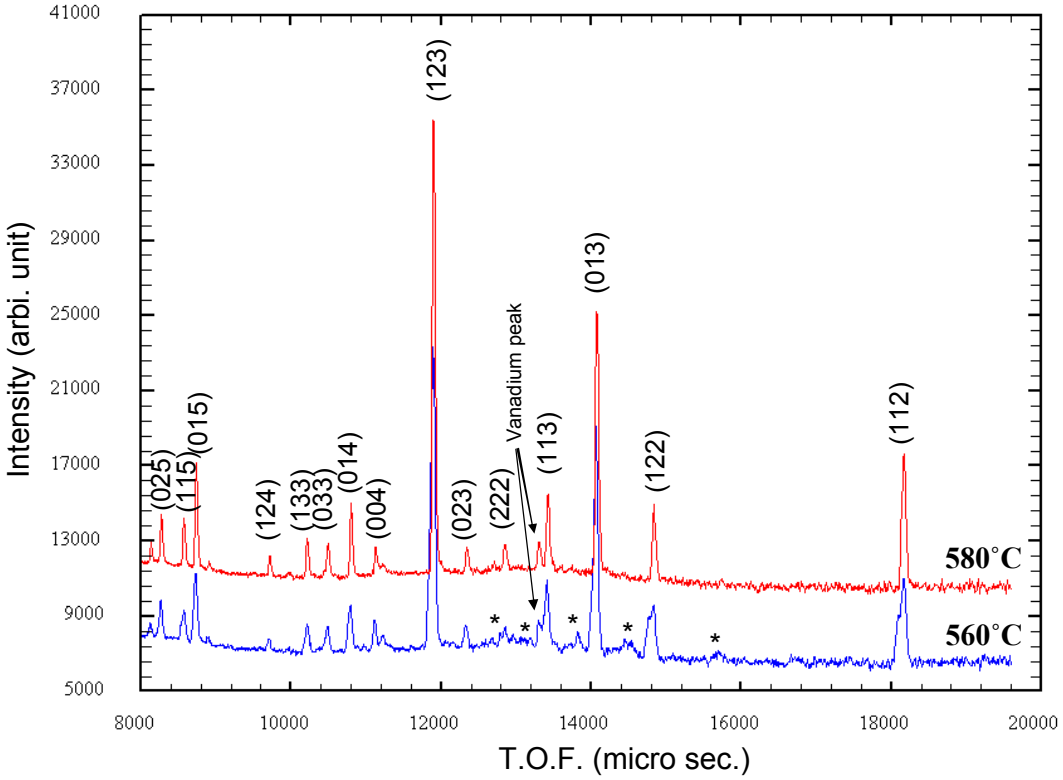
Intensity (arbi. unit)
T.O.F. (micro sec.)
41000
37000
33000
29000
25000
21000
17000
13000
9000
5000
8000
10000
12000
14000
16000
18000
20000
(025)
(115)
(015)
(124)
(133)
(033)
(014)
(004)
(123)
(023)
(222)
Vanadium peak
(113)
(013)
(122)
(112)
580˚C
560˚C
*

Fig. 3

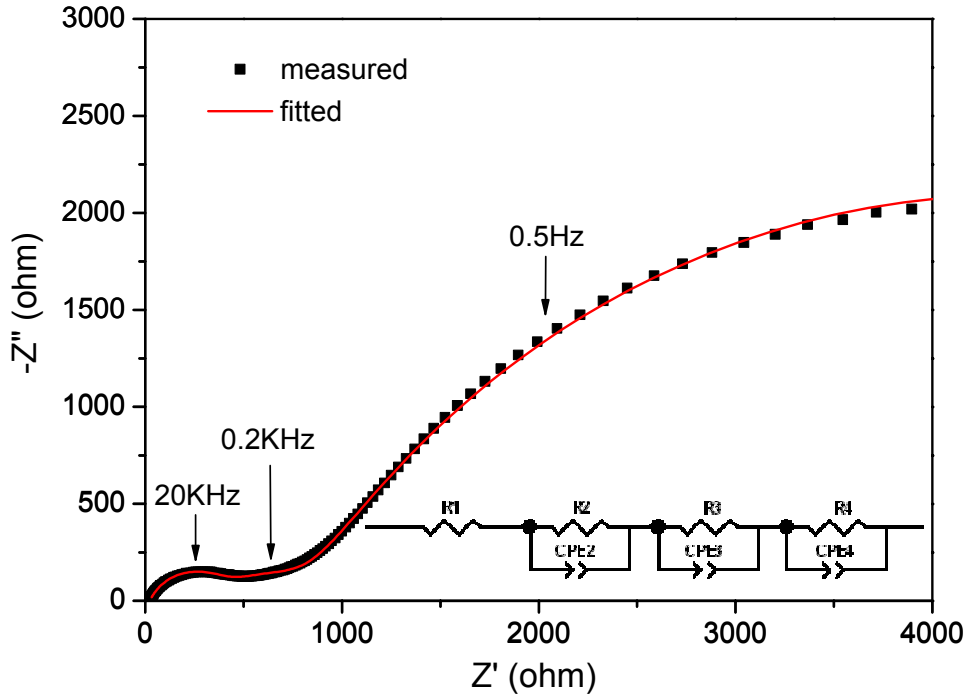
measured
fitted
0.5Hz
0.2KHz
20KHz
R1
R2
R3
R4
CPE2
CPE3
CPE4
-Z'' (ohm)
Z' (ohm)
0
500
1000
1500
2000
2500
3000
0
1000
2000
3000
4000

Fig. 4

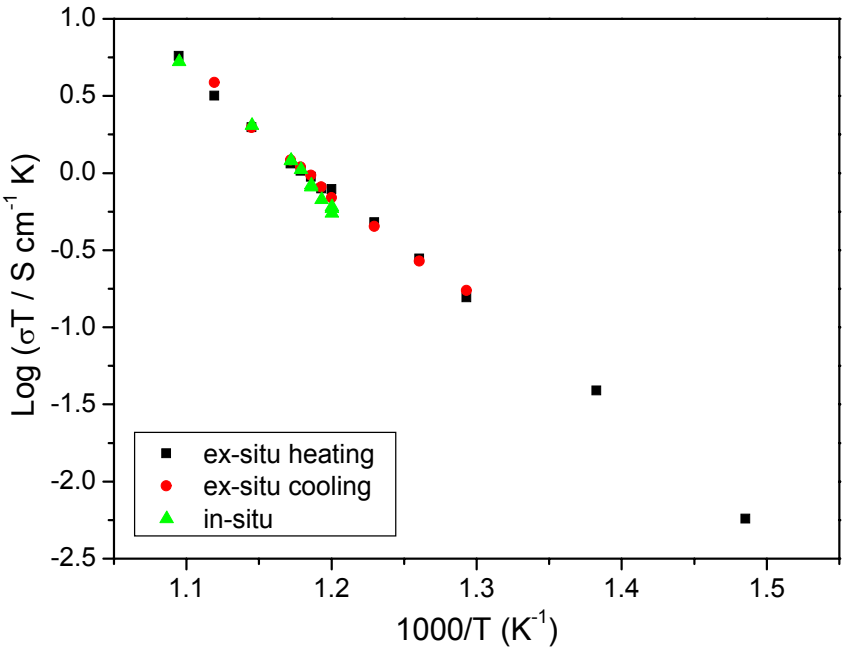
1.0
0.5
0.0
-0.5
-1.0
-1.5
-2.0
-2.5
Log (σT / S cm-1 K)
1.1
1.2
1.3
1.4
1.5
1000/T (K-1)
ex-situ heating
ex-situ cooling
in-situ

Fig. 5

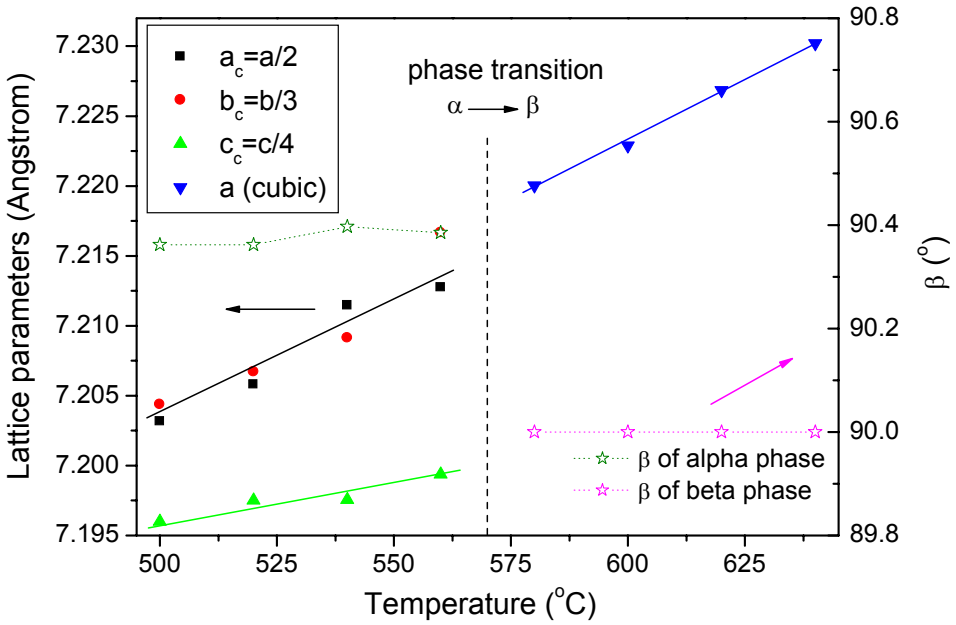
Lattice parameters (Angstrom)
7.230
7.225
7.220
7.215
7.210
7.205
7.200
7.195
500
525
550
575
600
625
Temperature (°C)
90.8
90.6
90.4
90.2
90.0
89.8
β (°)
a_c=a/2
b_c=b/3
c_c=c/4
a (cubic)
phase transition
α → β
β of alpha phase
β of beta phase

Fig. 6

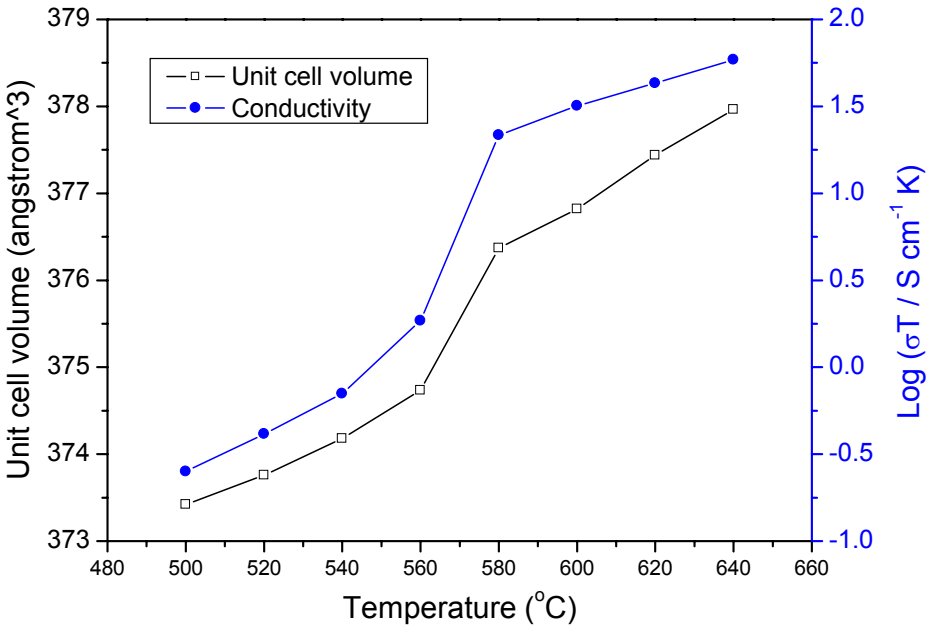
Unit cell volume
Conductivity
Unit cell volume (angstrom^3)
Log (σT / S cm^-1 K)
Temperature (°C)
379
378
377
376
375
374
373
2.0
1.5
1.0
0.5
0.0
-0.5
-1.0
480
500
520
540
560
580
600
620
640
660

Fig. 7

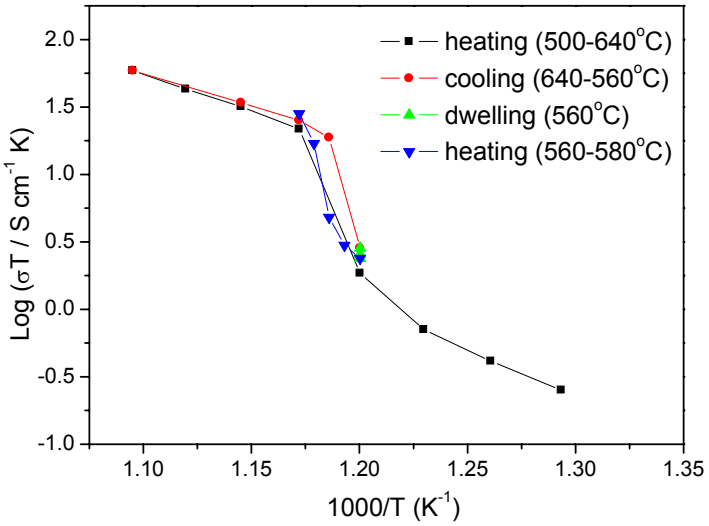
heating (500-640°C)
cooling (640-560°C)
dwelling (560°C)
heating (560-580°C)
Log (σT / S cm^{-1} K)
1000/T (K^{-1})
2.0
1.5
1.0
0.5
0.0
-0.5
-1.0
1.10
1.15
1.20
1.25
1.30
1.35

(a)

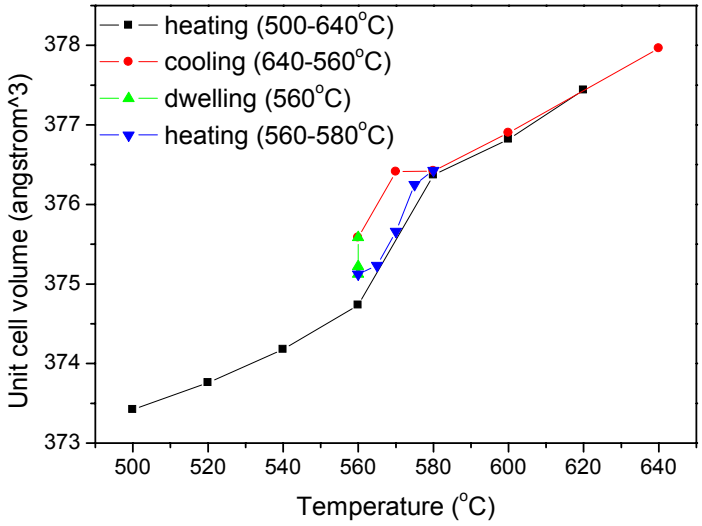
heating (500-640°C)
cooling (640-560°C)
dwelling (560°C)
heating (560-580°C)
Unit cell volume (angstrom^3)
Temperature (°C)
378
377
376
375
374
373
500
520
540
560
580
600
620
640

(b)